






Scattering of topological surface-state carriers at steps on surfaces

Naoya Fukui ^{1,*}, Rei Hobara,¹ Akari Takayama ^{1,†}, Ryota Akiyama ¹, Toru Hirahara ², and Shuji Hasegawa ¹

¹Department of Physics, University of Tokyo, 7-3-1 Hongo, Bunkyo-ku, Tokyo 113-0033, Japan

²Department of Physics, Tokyo Institute of Technology, 2-12-1 Ookayama, Meguro-ku, Tokyo 152-8551, Japan



(Received 29 April 2020; revised 31 July 2020; accepted 12 August 2020; published 17 September 2020)

The resistance across a step on ultrathin films of three different topological insulators, Bi_2Te_3 , Bi_2Se_3 , and $(\text{Bi}_{1-x}\text{Pb}_x)_2\text{Te}_3$, was measured through anisotropy in two-dimensional resistivity by using the *in situ* square four-point probe method in ultrahigh vacuum. The step resistance was much larger for Bi_2Te_3 than for Bi_2Se_3 in the range of 1–10 quintuple-layer thickness, due to the smaller critical thickness for isolation of topological surface states in Bi_2Te_3 . The transmission probability of carriers across a step is much higher for the bulk-insulating $(\text{Bi}_{1-x}\text{Pb}_x)_2\text{Te}_3$ than bulk-metallic Bi_2Te_3 , due to prevention of scattering of surface-state carriers into the bulk states. We were able to deduce microscopic information concerning the transmission probability at individual steps from the resistance data obtained macroscopically.

DOI: [10.1103/PhysRevB.102.115418](https://doi.org/10.1103/PhysRevB.102.115418)

I. INTRODUCTION

Topological insulators (TIs) have been attracting much attention due to their features such as topological surface states (TSSs), which are protected by the topological nature of electronic bulk states [1–4]. TSSs of three-dimensional TIs (3DTIs) have an outstanding feature, called spin-momentum locking, in which the spin direction of an electronic state is perpendicular to its momentum [3,5–7]. Theoretical studies predict that the spin-momentum locking suppresses the backscattering and even forbids the 180° backscattering of TSS carriers [8,9]. This nature is important not only for basic science but also for application to spintronics devices utilizing the charge and spin transport robust against disorders. The experimental demonstration of the backscattering suppression in 3DTIs has been also challenging and performed by employing scanning tunneling microscopy/spectroscopy (STM/STS). Observation of electronic states (quasiparticle interference patterns) around disorders, point defects, and atomic steps on TIs has shown that the backscattering at such disorders is indeed suppressed in many TIs, but the degree of the suppression varies among the TIs [10–13]. Detailed research has elucidated that the suppression of the backscattering is degraded by the coexisting bulk states, to which TSS carriers are allowed to be scattered.

Even though many TIs have been explored with STS since their discovery, it is only recently that the influence of backscattering suppression on electrical conduction has been investigated [14–16]. These works reported the step resistance on 3DTIs by the scanning tunneling potentiometry (STP)

technique and revealed that the step resistance governs the whole resistance of the TI surface. However, it still has not been clear to what extent the suppression of the backscattering affects the step resistance on 3DTIs. If the step resistance on TIs is really reflecting the suppression of backscattering, it should vary according to the degree of the backscattering suppression, which has not yet been investigated systematically.

In this paper, we measured the resistance across an atomic step on 3DTIs by the square four-point probe resistance measurement method. The 3DTI thin films were grown on a vicinal substrate to align the direction of atomic steps in a specific direction. The stepped *n*-type Bi_2Te_3 films exhibited anisotropic electrical conduction because the current flowing perpendicular to the steps experienced more atomic steps than that flowing parallel to the steps. On the other hand, *n*-type Bi_2Se_3 exhibited only a lower anisotropy, which implies a larger contribution from bulk states than in *n*-type Bi_2Te_3 . We also measured step resistivity of bulk-insulating $(\text{Bi}_{0.8}\text{Pb}_{0.2})_2\text{Te}_3$ to quantitatively evaluate the transmission probability of TSS carriers through a step. These results indicate that the topological transition due to hybridization of TSSs between the front and back surfaces of the film and the existence of bulk states at the Fermi level (E_F) enhances the backscattering, which is consistent with previous STS experiments and theoretical studies.

II. EXPERIMENTAL

The substrates were cut out of a vicinal Si(111) wafer with a 0.9° miscut from the (111) toward the $\langle\bar{1}\bar{1}2\rangle$ orientation. Its resistivity was 1.5–5 $\Omega\text{ cm}$ at room temperature (*n* type, P doped). When a flat Si(111) substrate is used, the atomic steps will be induced without any preference in three equivalent crystal orientations on the surface of TIs and the anisotropic resistance is averaged out in the macroscopic measurements [Fig. 1(a)]. On the other hand, when a vicinal Si(111) substrate is used, the steps will be introduced mostly in the $\langle\bar{1}\bar{1}0\rangle$

*n-fukui@rs.tus.ac.jp; Research Institute for Science and Technology, Tokyo University of Science, 2461 Yamazaki, Noda, Chiba 278-8510, Japan.

†Present address: Department of Physics, Waseda University, 3-4-1 Ohkubo, Shinjuku-ku, Tokyo 169-8555, Japan.

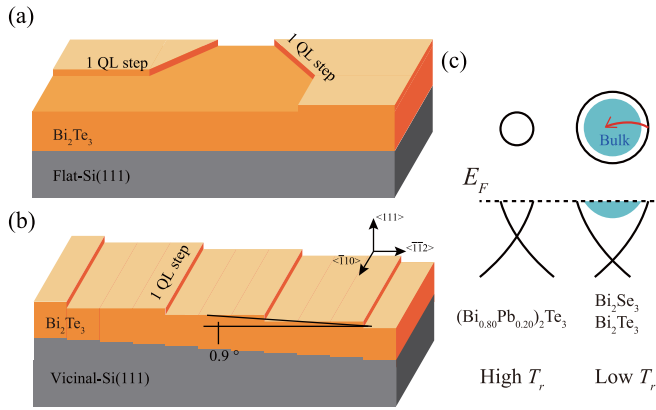


FIG. 1. Typical morphology of a thin film (a) grown on a flat silicon substrate and (b) on a vicinal substrate. (c) Schematic illustration of Fermi surfaces and band dispersions of the topological insulators examined in this work. Red arrows indicate scattering paths from a TSS to a bulk state.

direction and the step resistance appears as anisotropy in sheet conductivity [Fig. 1(b)].

First, a Si(111)- 7×7 superstructure was prepared by the special Joule heating process mentioned in Ref. [17] to avoid the step bunching. Next we prepared three types of TIs on the vicinal substrate: Pb-doped Bi_2Te_3 without bulk states at E_F , and as-grown (n type) Bi_2Te_3 and Bi_2Se_3 with bulk states at E_F [Fig. 1(c)]. Bi_2Te_3 thin films were grown on the Si(111)- 7×7 surface heated at 200°C by codepositing Bi and Te. Pb-doped Bi_2Te_3 , $(\text{Bi}_{1-x}\text{Pb}_x)_2\text{Te}_3$ ($x = 0.17, 0.20$), thin films were likewise grown by codepositing Bi, Pb, and Te. The ratios of the deposition rates of Bi, Pb, and Te were $1 - x$, x , and 20, respectively. Bi_2Se_3 thin films were grown on a Si(111)- $\beta\sqrt{3} \times \sqrt{3}$ -Bi surface heated at 200°C under the flux ratio Bi : Se $\sim 1 : 20$ [18]. We estimated the deposition rate of Bi from the formation of Si(111)- $\beta\sqrt{3} \times \sqrt{3}$ -Bi [19] and that of Pb from Si(111)-SiC-Pb [20]. Those of Se and Te were estimated by assuming that the disappearance of Si(111)- 7×7 spots in the reflection high energy electron diffraction (RHEED) pattern corresponds to the monolayer coverage. The RHEED patterns from all of the grown films indicated epitaxial growth of single-crystalline films with the (111) face on top [21]. The electrical conduction measurements and the sample preparation were performed *in situ* under ultrahigh vacuum in the temperature-variable four-tip STM chamber [22]. The tips were made of a tungsten wire by the dynamic electrochemical-etching technique [23]. The four tips were independently driven laterally and vertically by piezoelectric actuators to achieve arbitrary tip configurations under a scanning electron microscope (SEM). The thickness dependence measurements were done at room temperature while the temperature dependence measurements were performed from 6 K to 200 K.

III. RESULTS AND DISCUSSION

A. Bi_2Te_3 and Bi_2Se_3

In the films prepared on the vicinal substrate, steps in units of one quintuple layer (QL) height will be naturally introduced

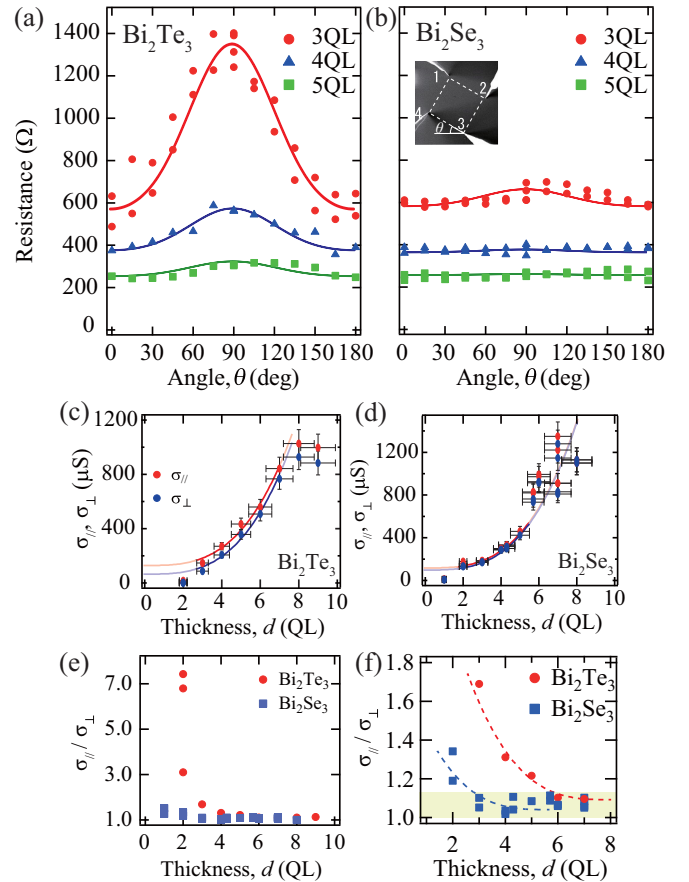


FIG. 2. (a), (b) The dependences of S4PP resistance on the rotation angle θ at room temperature for 3 QL, 4 QL, and 5 QL thick $\text{Bi}_2\text{Te}_3(111)$ films and $\text{Bi}_2\text{Se}_3(111)$ films on vicinal substrates, respectively. The solid lines are fitting curves reproduced by Eq. (1). The inset in (b) shows an SEM image under the measurement with the tip number and the illustration of the definition of θ . Atomic steps run horizontally in the image. (c), (d) The dependences of 2D electrical conductivity of the Bi_2Te_3 and Bi_2Se_3 thin film on their thicknesses. The solid lines are cubic to the thickness, drawn as guides to the eye. For both markers and lines, red and blue correspond to the cases parallel to and perpendicular to the atomic steps, respectively. (e), (f) The dependences of the conductivity anisotropy $\sigma_{\parallel}/\sigma_{\perp}$ of Bi_2Te_3 (red circles) and Bi_2Se_3 (blue boxes) on the film thickness. (f) is the magnification of (e). The dashed lines are guides to the eye.

on the film along the steps aligning on the substrate. Then the current flowing perpendicular to the steps undergoes more steps than in the case of step-parallel current, where the resistance is smaller than in the former case. As a result, the film will exhibit anisotropic sheet resistivity, which is suitable for detecting by the square four-point probe (S4PP) method [24,25]. The four tips were arranged in a square with a side length of $50 \mu\text{m}$ rotated by an angle θ with respect to the $\langle 110 \rangle$ direction that is the step-array direction [inset in Fig. 2(b)], and the S4PP resistance was measured as a function of θ . The S4PP resistance is defined as the voltage between tip 2 and tip 1 divided by the current flowing between tip 3 and tip 4.

First we measured the resistance of Bi_2Te_3 and Bi_2Se_3 films with various thicknesses shown in Figs. 2(a) and 2(b), respectively. It smoothly became larger from $\theta = 0^\circ$ (current applied along the steps) to $\theta = 90^\circ$ (perpendicular to the steps) and became smaller again toward $\theta = 180^\circ$. This is a typical behavior in anisotropic 2D systems as reported previously [14,24,26,27]. We can naturally conclude that the anisotropy of the films comes from the 1-QL-high steps induced by the vicinal substrate.

We first focus on Bi_2Te_3 films. For 3 QL thick Bi_2Te_3 , the mountain-shaped graph shows that the influence of atomic steps on the electrical resistivity is dominant at this thickness. For the thicker Bi_2Te_3 films, 4 QL and 5 QL, one can find two things. One is that the thicker film has a smaller S4PP resistance. If the TSSs are the dominant conduction channels, the resistance is independent of the thickness. Therefore the result shows that the S4PP resistance contains the contribution from bulk states, which are dominant in thicker films. The other finding is that the conduction anisotropy is smaller in the thicker films. In other words, the anisotropy caused by steps on the film surface is hindered by bulk conduction channels.

To evaluate the anisotropy, the following formula is convenient [24,26]:

$$R(\theta) = \frac{\sqrt{\rho_{\parallel}\rho_{\perp}}}{4\pi} \ln \frac{(\frac{\rho_{\perp}}{\rho_{\parallel}} + 1)^2 - 4(\frac{\rho_{\perp}}{\rho_{\parallel}} - 1)^2 \cos^2\theta \sin^2\theta}{(\sin^2\theta + \frac{\rho_{\perp}}{\rho_{\parallel}} \cos^2\theta)^2}, \quad (1)$$

where ρ_{\parallel} and ρ_{\perp} are the 2D resistivity along and across the step directions, respectively. The S4PP resistance was well reproduced by the fitting curves as shown by the solid curves in Fig. 2(a). For example, for a 3 QL film, $\rho_{\parallel} = 6.8 \text{ k}\Omega/\square$ and $\rho_{\perp} = 11.5 \text{ k}\Omega/\square$. The 2D conductivities σ_{\parallel} and σ_{\perp} , which are the inverses of ρ_{\parallel} and ρ_{\perp} , respectively, are obtained for each thickness and plotted in Fig. 2(c). In addition, the ratio between the two, $\rho_{\perp}/\rho_{\parallel} = \sigma_{\parallel}/\sigma_{\perp}$, were plotted in Figs. 2(e) and 2(f). The conductivity increasing with the thickness shows the bulk contribution to the electrical conduction. The increase in the conductivity was especially remarkable from 2 to 3 QL, where TSSs are likely to hybridize each other between the front and back surfaces of the Bi_2Te_3 film, whose critical thickness is 2 QL [28]. Probably for the same reason, $\sigma_{\parallel}/\sigma_{\perp}$ steeply dropped from 2 to 3 QL and gradually decreased with the thickness, and saturated to unity around 6 QL. The Bi_2Te_3 films thicker than 6 QL are dominated by bulk conduction.

Similarly to the Bi_2Te_3 films, the S4PP resistance of the Bi_2Se_3 films became larger with decreasing film thickness [Figs. 2(b) and 2(d)]. In contrast to the Bi_2Te_3 cases, only a marginal anisotropy was observed in S4PP resistance of vicinal Bi_2Se_3 films. The anisotropy ratio $\rho_{\perp}/\rho_{\parallel}$ is almost unity over all the thickness range above 2 QL, in contrast to the anisotropy of Bi_2Te_3 films [Fig. 2(f)]. This behavior implies a stronger contribution from the bulk states in the Bi_2Se_3 films.

The dependences of the conductivity, σ_{\parallel} and σ_{\perp} , on the film thickness were similar to each other for Bi_2Te_3 and Bi_2Se_3 [Figs. 2(c) and 2(d)]. Both σ_{\parallel} and σ_{\perp} of Bi_2Te_3 and Bi_2Se_3 increase with the thickness. This shows that not only the TSSs but also the bulk states contribute to the

conductivity. The nonlinear dependence of conductivity on the film thickness [Figs. 2(c) and 2(d)] also implies the existence of a quantum effect due to the confinement in the direction of the thickness and scattering at the film surface. This phenomenon is widely seen in every sort of material when its thickness is thin enough [29–31]. Contrary to the similar thickness dependence of the conductivity between Bi_2Te_3 and Bi_2Se_3 , the thickness dependence of the anisotropy in conductivity, $\sigma_{\parallel}/\sigma_{\perp}$, is different between them. The conductivity anisotropy decreased with the increasing thickness up to 6 QL in Bi_2Te_3 films and disappeared beyond 6 QL. On the other hand, in Bi_2Se_3 films, we did not find significant anisotropy in the range of thicknesses examined [Fig. 2(e)].

This difference of conductivity anisotropy between Bi_2Te_3 and Bi_2Se_3 can be attributed to not only the difference in the nature of Bi_2Te_3 and Bi_2Se_3 themselves but also the difference of the interfaces: the Te wetting layer was an ill-ordered interface between Bi_2Te_3 and the substrate while a well-ordered $\text{Si}(111)\text{-}\beta\text{-}\sqrt{3} \times \sqrt{3}\text{-Bi}$ was the interface between Bi_2Se_3 and the substrate [18,32]. However, the influence of the interface in this work seems to be limited judging from the conductivity of the thinnest film of Bi_2Te_3 or Bi_2Se_3 . In this thickness range, the conductivity was around $10 \mu\text{S}/\square$; therefore the conductivity of the interface is at most $10 \mu\text{S}/\square$. On the other hand, the conductivity difference between along and across the steps is around $100 \mu\text{S}/\square$, which means the conductivity anisotropy takes place dominantly in the film, not at the interface. The difference of conductivity anisotropy between Bi_2Te_3 and Bi_2Se_3 should be explained by the difference in their nature. The most possible explanation is the difference in property of TSSs between Bi_2Te_3 and Bi_2Se_3 . Generally speaking, every TI film has a critical thickness beyond which gapless TSSs start to appear. A topological insulator film thinner than its critical thickness is known to show an energy gap opening at the Dirac point due to hybridization of TSSs at the front and back surfaces of the film, resulting in diminishing typical properties of topological insulators such as two-dimensionality and a long mean-free path [33,34]. Since the critical thickness of Bi_2Te_3 is 2 QL [28], in the thickness range of 2–5 QL where the TSSs on both surfaces are well separated from each other, we can say that the remarkable anisotropy is caused by TSSs. Although the conductivity is thought of as a sum of those of TSSs and the bulk states, the former has anisotropy due to the surface steps while the latter is isotropic due to less influence of the surface steps. The isotropic conduction of thicker Bi_2Te_3 films can be attributed to the dominant contribution of the bulk states.

The critical thickness of Bi_2Se_3 , on the other hand, is 6 QL [21,35]. As mentioned above, Bi_2Se_3 films of 2–5 QL were almost isotropic. By taking into consideration that this thickness range is below the critical thickness, we can explain this isotropic conduction by hybridization effect as mentioned below. The TSSs of Bi_2Se_3 films thinner than its critical thickness hybridize with the TSSs on the opposite surface to open the energy gap. The TSSs consequently cannot be distinguished from the bulk states, but rather behave as a conduction channel delocalized in the direction of thickness. Therefore the influence of the surface steps was marginal. When the thickness is thicker than 5 QL, the TSSs appear separately on the front and back surfaces of the film. However,

the conductivity of the whole film is isotropic since the contribution of bulk is already dominant.

Finally we note the influence of the warping effect on the step resistance. Bi_2Te_3 undergoes the warping effect, which deforms the Fermi surface of TSSs into a hexagonal shape, more strongly than Bi_2Se_3 does [36,37]. The warped Fermi surface enhances the backscattering of TSS carriers as investigated theoretically and experimentally [8–11]. This fact seemingly explains our results that Bi_2Te_3 films are more strongly affected by the surface steps than Bi_2Se_3 films. However, this explanation is valid only when the conductivity of bulk states is the same between Bi_2Te_3 and Bi_2Se_3 . The control of the bulk state conduction is required for the accurate discussion about the influence of the warping effect.

B. $(\text{Bi}_{1-x}\text{Pb}_x)_2\text{Te}_3$

We have thus revealed the influence of TSSs on the electric conduction by comparing two different TI materials. Nevertheless, the existence of bulk states made the situation complicated and we have only given a qualitative explanation. For a quantitative evaluation of step resistance, we need to eliminate the bulk conduction channels. Hence, we next measured the vicinal Pb-doped Bi_2Te_3 films. The Pb atoms as hole dopants compensate the doped electrons by Te vacancies and the Fermi level is tuned within the bulk band gap [38]. Therefore this is the simplest system to discuss the electron transport property of TSSs. Figure 3(a) shows the RHEED pattern of the 3 QL thick $(\text{Bi}_{0.80}\text{Pb}_{0.20})_2\text{Te}_3$ thin film grown on the vicinal Si(111) substrate. The sharp diffraction streaks indicate the high quality of the film. The spot interval of $(\text{Bi}_{0.80}\text{Pb}_{0.20})_2\text{Te}_3$ is identical with that of Bi_2Te_3 within the errors, which means that the $(\text{Bi}_{0.80}\text{Pb}_{0.20})_2\text{Te}_3$ thin film has the same atomic structure as Bi_2Te_3 except 20% substitution of Pb for Bi.

Figure 3(b) is the S4PP resistance of the vicinal 3 QL $(\text{Bi}_{0.80}\text{Pb}_{0.20})_2\text{Te}_3$ film at 6 K. Anisotropy in S4PP resistance is clearly observed. Using Eq. (1), we have obtained the sheet resistivity parallel to the steps $\rho_{\parallel} = 4.2 \text{ k}\Omega/\square$ and that perpendicular to the steps $\rho_{\perp} = 7.7 \text{ k}\Omega/\square$ for this film at 6 K.

Figure 3(c) shows the temperature dependence of ρ_{\parallel} and ρ_{\perp} . Both resistivities gradually increase as the temperature becomes higher. This metallic behavior eliminates the possibility that the anisotropy was caused by the bulk silicon substrate or its surface space charge layer, because of freeze-out of carriers there. Furthermore, the resistivity difference between the two directions maintains its magnitude around $4 \text{ k}\Omega$ throughout the measurement temperature range (see Fig. S1 in the Supplemental Material [39]). This behavior suggests that the anisotropy is caused by elastic scatterings of carriers, most probably by atomic steps in this case, not by inelastic scattering by phonons. Similar behaviors have been observed in other systems where some defects were anisotropically introduced [40,41]. Consequently the difference of the resistivity in the two directions is attributed to the step resistance, which is caused by elastic scattering which is temperature-independent. The resistivity ρ_{\perp} in the $\langle\bar{1}\bar{1}2\rangle$ direction is naturally regarded as a series of the resistance of terraces and steps while the resistivity ρ_{\parallel} in the

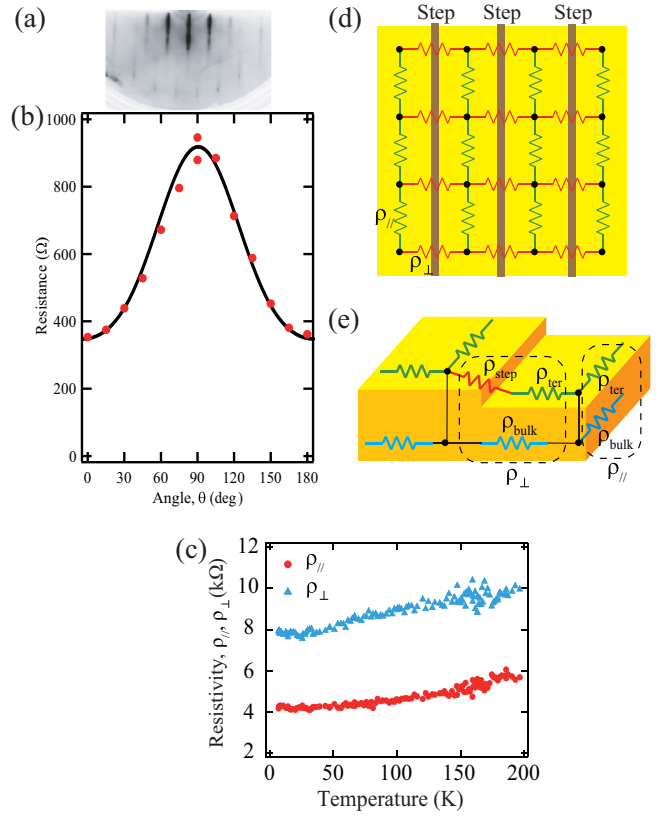


FIG. 3. (a) The RHEED pattern of $(\text{Bi}_{0.80}\text{Pb}_{0.20})_2\text{Te}_3$ 3 QL film. (b) The dependence of S4PP resistance of 3 QL $(\text{Bi}_{0.80}\text{Pb}_{0.20})_2\text{Te}_3$ on the rotation angle θ measured at 6 K. (c) The temperature dependences of the resistivity of the 3 QL thick $(\text{Bi}_{0.80}\text{Pb}_{0.20})_2\text{Te}_3$ thin film along (the red circles) and across (the blue triangles) the steps. (d), (e) Schematic illustrations of the electrical conduction in a vicinal topological insulator film with atomic steps (d) from the top view and (e) the side view. Equivalent circuits are overlapped.

$\langle 1\bar{1}0\rangle$ direction mainly comes from the terraces [Figs. 3(d) and 3(e)].

In general, the conductivity σ of a thin film grown on a substrate is expressed as the sum of parallel conduction channels,

$$\sigma = \sigma_{\text{film}} + \sigma_{\text{sub}} + \sigma_{\text{int}} + \sigma_{\text{sc}}, \quad (2)$$

where σ_{film} , σ_{sub} , σ_{int} , and σ_{sc} are the conductivity of the film, the substrate, the interface between them, and the space charge layer under the film, respectively. The anisotropic conductivity of $(\text{Bi}_{0.80}\text{Pb}_{0.20})_2\text{Te}_3$ film on a vicinal substrate is caused by the anisotropy in those conduction channels between the two directions. First of all, σ_{sub} and σ_{sc} can be ignored since these components will become zero due to the carrier freeze-out when the temperature is lowered as mentioned before. σ_{int} is the contribution from the tellurium wetting layer between the $(\text{Bi}_{0.80}\text{Pb}_{0.20})_2\text{Te}_3$ film and the substrate. A previous work reported that the conductivity of Te/Si(111)-7 \times 7 was on the order of $10 \mu\text{S}/\square$, which is smaller than 10% of the anisotropy of the $(\text{Bi}_{0.80}\text{Pb}_{0.20})_2\text{Te}_3$ film on a vicinal substrate [42]. We conclude that the interface does not play an important role in the conductivity anisotropy

in the stepped $(\text{Bi}_{0.80}\text{Pb}_{0.20})_2\text{Te}_3$ film and that the stepped film itself causes the conductivity anisotropy.

The conductivity of a topological insulator film is composed of three conduction channels [43],

$$\sigma_{\text{film}} = \sigma_{\text{top}} + \sigma_{\text{bulk}} + \sigma_{\text{bot}}, \quad (3)$$

where σ_{top} , σ_{bulk} , and σ_{bot} are the conductivity of the top surface, the bulk, and the bottom surface, respectively. Among them, σ_{bulk} can be regarded as zero at low temperature because $(\text{Bi}_{0.80}\text{Pb}_{0.20})_2\text{Te}_3$ is a bulk insulating topological insulator with its Fermi energy in the bulk band gap. Therefore, we can conclude that the anisotropy of the conductivity takes place in the top and bottom surfaces due to the atomic steps existing there,

$$\sigma_{\parallel} = \rho_{\parallel}^{-1} = \sigma_{\parallel,\text{top}} + \sigma_{\parallel,\text{bot}}, \quad (4)$$

$$\sigma_{\perp} = \rho_{\perp}^{-1} = \sigma_{\perp,\text{top}} + \sigma_{\perp,\text{bot}}, \quad (5)$$

where the subscripts \parallel and \perp describe the direction parallel to and perpendicular to the atomic steps, respectively. Because the conductivity parallel to and perpendicular to the steps is different by the step resistance,

$$\rho_{\parallel,\text{top}} = \sigma_{\parallel,\text{top}}^{-1} = \rho_{\text{ter,top}}, \quad (6)$$

$$\rho_{\perp,\text{top}} = \sigma_{\perp,\text{top}}^{-1} = \rho_{\text{ter,top}} + N_{\text{step,top}}\rho_{\text{step,top}}, \quad (7)$$

$$\rho_{\parallel,\text{bot}} = \sigma_{\parallel,\text{bot}}^{-1} = \rho_{\text{ter,bot}}, \quad (8)$$

$$\rho_{\perp,\text{bot}} = \sigma_{\perp,\text{bot}}^{-1} = \rho_{\text{ter,bot}} + N_{\text{step,bot}}\rho_{\text{step,bot}}, \quad (9)$$

where $\rho_{\text{ter,top(bot)}}$ is the resistivity of the terrace on the top (bottom) surface and $\rho_{\text{step,top(bot)}}$ is the resistance across a single step on the top (bottom) surface per unit length of the step. $N_{\text{step,top(bot)}}$ is the step density, the number of steps crossing a unit length on the top (bottom) surface [26]. The expressions above are the most general ones. For simplification of the discussion, the values for the top and bottom surfaces are regarded as the same, for example, $\rho_{\text{ter,top}} = \rho_{\text{ter,bot}}$. Finally ρ_{\parallel} and ρ_{\perp} are written as

$$\rho_{\parallel} = \frac{1}{2}\rho_{\text{ter,top}}, \quad (10)$$

$$\rho_{\perp} = \frac{1}{2}\rho_{\text{ter,top}} + \frac{1}{2}N_{\text{step,top}}\rho_{\text{step,top}}. \quad (11)$$

Because the film was grown on the vicinal substrate with 0.9° miscut off (111), $N_{\text{step,top}}$ should fulfill the relation $h_{\text{QL}}N_{\text{step,top}} = \tan 0.9^\circ$ to compensate the miscut of the substrate, where h_{QL} is the height of 1 QL and equals 1.016 nm [44]. This kind of growth actually takes place in Bi_2Se_3 films grown on a vicinal Si(111) substrate as shown in the supplemental information of Ref. [14]. Therefore, the step density was estimated as $N_{\text{step}} = 1.456 \times 10^5 \text{ cm}^{-1}$. By inserting all the values above into Eqs. (10) and (11), the resistivity across a single step $\rho_{\text{step}} = 4.8 \times 10^{-2} \Omega \text{ cm}$ is obtained. For comparison, the resistivity across a single step of Bi_2Se_3 and $(\text{Bi}_{0.53}\text{Sb}_{0.47})_2\text{Te}_3$ obtained by STP is on the order of $10^{-3} \Omega \text{ cm}$ [14,15], which is smaller by one order of magnitude than ours. This difference may come from the conduction through the bulk states existing at E_F in the sample of the previous studies because they were done at

room temperature, resulting in lowering the step resistance apparently.

The step resistivity contains the information of the transmission probability of a carrier across the step. According to Ref. [26], the step resistivity is written by the following form,

$$\rho_{\text{step}} = \frac{h}{e^2} \frac{\pi}{k_F} \frac{1 - T_r}{T_r}, \quad (12)$$

where h is the Planck constant and e is the elementary charge. k_F is the Fermi wave number of the topological surface state. T_r is the transmission probability that the carriers transmit through the step. Note that this formula is different from that in Ref. [26] by a factor 2 due to the contributions from the top and bottom surfaces of the film and that we have taken a formula for four-terminal form about the T_r [45]. The transmission probability of $(\text{Bi}_{0.80}\text{Pb}_{0.20})_2\text{Te}_3$, $T_r = 0.25$, was obtained from $k_F = 0.05 \text{ \AA}^{-1}$ reported by the previous angle-resolved photoemission spectroscopy (ARPES) measurements of $(\text{Bi}_{0.78}\text{Pb}_{0.22})_2\text{Te}_3$ [38].

We also performed the same experiments and analysis to obtain $T_r = 0.32$ for another sample, $(\text{Bi}_{0.83}\text{Pb}_{0.17})_2\text{Te}_3$, whose bulk states are also eliminated from E_F (Fig. S2 in the Supplemental Material [39] and Table I). Here we can say that the transmission probability of TSS carriers at steps on $(\text{Bi}_{1-x}\text{Pb}_x)_2\text{Te}_3$ typically takes a value from $\frac{1}{4}$ to $\frac{1}{3}$. The fact that more than half of the TSS carriers were reflected by an atomic step does not seem consistent with the suppressed backscattering expected as a general feature of TSSs. Actually these values are comparable to the transmission probability at an atomic step on $\text{Si}(111)\text{-}\sqrt{3} \times \sqrt{3}\text{-Ag}$, a topologically trivial metallic monolayer system, obtained from similar electrical conductivity measurements [26]. The experimentally determined transmission probability for the $\text{Si}(111)\text{-}\sqrt{3} \times \sqrt{3}\text{-Ag}$ surface was consistent with the theoretical estimation under the assumption that the step is regarded as a potential barrier with the height of its work function. If the same assumption is applied to $(\text{Bi}_{1-x}\text{Pb}_x)_2\text{Te}_3$ surface states, T_r should not be less than $\frac{2}{3}$ because of Klein tunneling, which is inconsistent with the present experiment [46,47]. A possible explanation to this discrepancy is the carrier scattering from the top to the bottom TSSs or vice versa. This scattering is not forbidden even under the topological protection based on time-reversal symmetry. Since the film thickness is 3 QL and the two TSSs at the top and bottom surfaces are spatially close, this scattering channel may weaken the expected suppression of backscattering.

The analysis procedure above for obtaining ρ_{step} and T_r is applicable only to the system where bulk conduction channels are suppressed. However, it is formally applicable to the as-prepared Bi_2Te_3 film to give the lower limit of ρ_{step} and the upper limit of the transmission probability. In 3 QL Bi_2Te_3 , $\rho_{\text{step}} = 6 \times 10^{-3} \Omega \text{ cm}$ and $T_r = 0.07$. Actually, the former is underestimated and the latter is overestimated due to the bulk states, which provide another channel for carriers. In the case of 3 QL Bi_2Se_3 , formal T_r is almost unity, implying large contribution from the bulk states. Nominal values of $T_r \approx 1$ are also the case with Bi_2Se_3 with another thickness and thicker Bi_2Te_3 , which is consistent with previous studies

TABLE I. The parameters of the topological insulator films investigated in this paper. The thickness of each film is 3 QL.

	$\sigma_{s\parallel}$ (μS)	$\sigma_{s\perp}$ (μS)	ρ_{step} ($\Omega\text{ cm}$)	T_r	TSS k_F (\AA^{-1})	Notes	Reference
$(\text{Bi}_{0.80}\text{Pb}_{0.20})_2\text{Te}_3$	240 ± 20	130 ± 10	4.8×10^{-3}	0.25	0.050	Bulk insulating, 6 K	[38]
$(\text{Bi}_{0.83}\text{Pb}_{0.17})_2\text{Te}_3$	210 ± 20	140 ± 10	3.0×10^{-3}	0.32	0.056	Bulk insulating, 6 K	[38]
Bi_2Te_3	$<150 \pm 10$	$<90 \pm 10$	$>6 \times 10^{-3}$	<0.07	0.18	Bulk n type, RT	[28]
Bi_2Se_3	$<180 \pm 10$	$<170 \pm 10$			0.10	Bulk n type, RT	[21]

on 14 QL Bi_2Se_3 [14] and 9 QL Sb-doped Bi_2Te_3 [15] by microscopic STP measurements.

C. Carrier transmissivity through a step on topological insulators

Table I shows all the characteristic parameters obtained by the analyses above. T_r , which indicates how robust the carriers are against scattering at steps, varies from one to another. However, T_r tends to become higher in the TI films where the bulk states are eliminated from the Fermi surface. This is consistent with the condition that quasiparticle interference does not appear in STS measurements for such bulk-insulating TIs [48]. Standing on a different point of view, we can say that the quasiparticle interference observed in STS images is indeed a result of strong scattering of the surface electrons. The nature of scattering which can be investigated in the microscopic regime actually has an influence on electronic conduction and appears in a form of step resistance which is accessible by measurements in the macroscopic regime with four-probe conductivity measurements.

IV. CONCLUSION

In summary, we measured the electrical resistivity across the atomic steps on TI thin films grown on a vicinal substrate. We obtained the transmission probability of TSS carriers through a step for the bulk-insulating topological insulator $(\text{Bi}_{1-x}\text{Pb}_x)\text{Te}_3$, which is not significantly high compared with that of a topologically trivial metallic monolayer system. Even though the step resistance and corresponding transmission probability for Bi_2Te_3 and Bi_2Se_3 films were not directly obtained due to large contribution from bulk states, we found a detectable step resistance of Bi_2Te_3 films while negligible step resistance at Bi_2Se_3 films because the critical thickness is smaller in Bi_2Te_3 films than in Bi_2Se_3 films. The bulk states also hindered the influence of the TSS Fermi-surface warping effect on the electrical resistance.

ACKNOWLEDGMENTS

Our work was supported by Grants-in-Aid for Scientific Research No. 25246025 and No. 16H02108, and Grant-in-Aid for JSPS Fellows No. 13J01282.

- [1] C. L. Kane and E. J. Mele, *Phys. Rev. Lett.* **95**, 146802 (2005).
[2] L. Fu and C. L. Kane, *Phys. Rev. B* **74**, 195312 (2006).
[3] B. A. Bernevig, T. L. Hughes, and S.-C. Zhang, *Science* **314**, 1757 (2006).
[4] M. Z. Hasan and C. L. Kane, *Rev. Mod. Phys.* **82**, 3045 (2010).
[5] H. Zhang, C.-X. Liu, X.-L. Qi, X. Dai, Z. Fang, and S.-C. Zhang, *Nat. Phys.* **5**, 438 (2009).
[6] Z.-H. Pan, E. Vescovo, A. V. Fedorov, D. Gardner, Y. S. Lee, S. Chu, G. D. Gu, and T. Valla, *Phys. Rev. Lett.* **106**, 257004 (2011).
[7] S. Souma, K. Kosaka, T. Sato, M. Komatsu, A. Takayama, T. Takahashi, M. Kriener, K. Segawa, and Y. Ando, *Phys. Rev. Lett.* **106**, 216803 (2011).
[8] K. Kobayashi, *Phys. Rev. B* **84**, 205424 (2011).
[9] J. An and C. S. Ting, *Phys. Rev. B* **86**, 165313 (2012).
[10] T. Hanaguri, K. Igarashi, M. Kawamura, H. Takagi, and T. Sasagawa, *Phys. Rev. B* **82**, 081305(R) (2010).
[11] T. Zhang, P. Cheng, X. Chen, J.-F. Jia, X. Ma, K. He, L. Wang, H. Zhang, X. Dai, Z. Fang, X. Xie, and Q.-K. Xue, *Phys. Rev. Lett.* **103**, 266803 (2009).
[12] Z. Alpichshev, J. G. Analytis, J.-H. Chu, I. R. Fisher, Y. L. Chen, Z. X. Shen, A. Fang, and A. Kapitulnik, *Phys. Rev. Lett.* **104**, 016401 (2010).
[13] S. Kim, S. Yoshizawa, Y. Ishida, K. Eto, K. Segawa, Y. Ando, S. Shin, and F. Komori, *Phys. Rev. Lett.* **112**, 136802 (2014).
[14] S. Bauer and C. A. Bobisch, *Nat. Commun.* **7**, 11381 (2016).
[15] F. Lüpke, M. Eschbach, T. Heider, M. Lanius, P. Schüffegen, D. Rosenbach, N. von den Driesch, V. Cherepanov, G. Mussler, L. Plucinski, D. Grützmacher, C. M. Schneider and B. Voigtländer, *Nat. Commun.* **8**, 15704 (2017).
[16] S. Bauer and C. A. Bobisch, *J. Phys.: Condens. Matter* **29**, 334002 (2017).
[17] J.-L. Lin, D. Y. Petrovykh, J. Viernow, F. K. Men, D. J. Seo, and F. J. Himpsel, *J. Appl. Phys.* **84**, 255 (1998).
[18] G. Zhang, H. Qin, J. Teng, J. Guo, Q. Guo, X. Dai, Z. Fang, and K. Wu, *Appl. Phys. Lett.* **95**, 053114 (2009).
[19] K. J. Wan, T. Guo, W. K. Ford, and J. C. Hermanson, *Phys. Rev. B* **44**, 3471 (1991).
[20] K. Horikoshi, X. Tong, T. Nagao, and S. Hasegawa, *Phys. Rev. B* **60**, 13287 (1999).
[21] Y. Sakamoto, T. Hirahara, H. Miyazaki, S. I. Kimura, and S. Hasegawa, *Phys. Rev. B* **81**, 165432 (2010).
[22] N. Fukui, R. Hobara, T. Hirahara, S. Hasegawa, Y. Miyatake, H. Mizuno, T. Sasaki, and T. Nagamura, *e-J. Surf. Sci. Nanotechnol.* **12**, 423 (2014).
[23] R. Hobara, S. Yoshimoto, S. Hasegawa, and K. Sakamoto, *e-J. Surf. Sci. Nanotechnol.* **5**, 94 (2007).
[24] T. Kanagawa, R. Hobara, I. Matsuda, T. Tanikawa, A. Natori, and S. Hasegawa, *Phys. Rev. Lett.* **91**, 036805 (2003).

- [25] I. Miccoli, F. Edler, H. Pfnür, and C. Tegenkamp, *J. Phys.: Condens. Matter* **27**, 223201 (2015).
- [26] I. Matsuda, M. Ueno, T. Hirahara, R. Hobara, H. Morikawa, C. Liu, and S. Hasegawa, *Phys. Rev. Lett.* **93**, 236801 (2004).
- [27] N. Nagamura, R. Hobara, T. Uetake, T. Hirahara, M. Ogawa, T. Okuda, K. He, P. Moras, P. M. Sheverdyaeva, C. Carbone, K. Kobayashi, I. Matsuda, and S. Hasegawa, *Phys. Rev. B* **89**, 125415 (2014).
- [28] Y.-Y. Li, G. Wang, X.-G. Zhu, M.-H. Liu, C. Ye, X. Chen, Y.-Y. Wang, K. He, L.-L. Wang, X.-C. Ma, H.-J. Zhang, X. Dai, Z. Fang, X.-C. Xie, Y. Liu, X.-L. Qi, J.-F. Jia, S.-C. Zhang, and Q.-K. Xue, *Adv. Mater.* **22**, 4002 (2010).
- [29] L. He, F. Xiu, Y. Wang, A. V. Fedorov, G. Huang, X. Kou, M. Lang, W. P. Beyermann, J. Zou, and K. L. Wang, *J. Appl. Phys.* **109**, 103702 (2011).
- [30] T. Hirahara, I. Matsuda, S. Yamazaki, N. Miyata, and S. Hasegawa, *Appl. Phys. Lett.* **91**, 202106 (2007).
- [31] G. Fishman and D. Calecki, *Phys. Rev. Lett.* **62**, 1302 (1989).
- [32] T. Shirasawa, J. Tsunoda, T. Hirahara, and T. Takahashi, *Phys. Rev. B* **87**, 075449 (2013).
- [33] A. A. Taskin, S. Sasaki, K. Segawa, and Y. Ando, *Phys. Rev. Lett.* **109**, 066803 (2012).
- [34] N. Bansal, Y. S. Kim, M. Brahlek, E. Edrey, and S. Oh, *Phys. Rev. Lett.* **109**, 116804 (2012).
- [35] Y. Zhang, K. He, C.-Z. Chang, C.-L. Song, L.-L. Wang, X. Chen, J.-F. Jia, Z. Fang, X. Dai, W.-Y. Shan, S.-Q. Shen, Q. Niu, X.-L. Qi, S.-C. Zhang, X.-C. Ma, and Q.-K. Xue, *Nat. Phys.* **6**, 584 (2010).
- [36] Y. L. Chen, J. G. Analytis, J.-H. Chu, Z. K. Liu, S.-K. Mo, X. L. Qi, H. J. Zhang, D. H. Lu, X. Dai, Z. Fang, S. C. Zhang, I. R. Fisher, Z. Hussain, and Z.-X. Shen, *Science* **325**, 178 (2009).
- [37] K. Kuroda, M. Arita, K. Miyamoto, M. Ye, J. Jiang, A. Kimura, E. E. Krasovskii, E. V. Chulkov, H. Iwasawa, T. Okuda, K. Shimada, Y. Ueda, H. Namatame, and M. Taniguchi, *Phys. Rev. Lett.* **105**, 076802 (2010).
- [38] M. Aitani, Y. Sakamoto, T. Hirahara, M. Yamada, H. Miyazaki, M. Matsunami, S. Kimura, and S. Hasegawa, *Jpn. J. Appl. Phys.* **52**, 110112 (2013).
- [39] See Supplemental Material at <http://link.aps.org/supplemental/10.1103/PhysRevB.102.115418> for the detailed temperature dependence of ρ_{\parallel} and ρ_{\perp} of $(\text{Bi}_{1-x}\text{Pb}_x)_2\text{Te}_3$ films.
- [40] A. W. Tsen, L. Brown, M. P. Levendorf, F. Ghahari, P. Y. Huang, R. W. Havener, C. S. Ruiz-Vargas, D. A. Muller, P. Kim, and J. Park, *Science* **336**, 1143 (2012).
- [41] G. Moschetti, H. Zhao, P.-Å. Nilsson, S. Wang, A. Kalabukhov, G. Dambrine, S. Bollaert, L. Desplanque, X. Wallart, and J. Grah, *Appl. Phys. Lett.* **97**, 243510 (2010).
- [42] S. Just, F. Lüpke, V. Cherepanov, F. S. Tautz, and B. Voigtländer, *Phys. Rev. B* **101**, 245413 (2020).
- [43] F. Lüpke, S. Just, M. Eschbach, T. Heider, E. Młyńczak, M. Lanus, P. Schüffelgen, D. Rosenbach, N. von den Driesch, V. Cherepanov, G. Mussler, L. Plucinski, D. Grützmacher, C. M. Schneider, F. S. Tautz, and B. Voigtländer, *npj Quantum Mater.* **3**, 46 (2018).
- [44] C. H. Champness and A. L. Kipling, *Can. J. Phys.* **44**, 769 (1966).
- [45] S. Datta, *Electronic Transport in Mesoscopic Systems* (Cambridge University Press, Cambridge, 2002).
- [46] M. I. Katsnelson, K. S. Novoselov, and A. K. Geim, *Nat. Phys.* **2**, 620 (2006).
- [47] See Supplemental Material at <http://link.aps.org/supplemental/10.1103/PhysRevB.102.115418> for the derivation of the transmission probability of topological surface states.
- [48] S. Kim, M. Ye, K. Kuroda, Y. Yamada, E. E. Krasovskii, E. V. Chulkov, K. Miyamoto, M. Nakatake, T. Okuda, Y. Ueda, K. Shimada, H. Namatame, M. Taniguchi, and A. Kimura, *Phys. Rev. Lett.* **107**, 056803 (2011).